A discontinuous model of exchange rate dynamics with sentiment traders

Giovanni Campisi[1], Anastasiia Panchuk[2*] and Fabio Tramontana[3]

[1]Polytechnic University of Marche, Italy.
[2*]Institute of Mathematics NASU, Ukraine.
[3]University of Urbino, Italy.

*Corresponding author(s). E-mail(s): anastasiia.panchuk@gmail.com;
Contributing authors: giovannicampisi6@gmail.com; fabio.tramontana@uniurb.it;

Abstract

In the present paper, we investigate the complex dynamics arising from a behavioral exchange rate discontinuous model with heterogeneous agents. Unlike previous works explaining the emergence of chaos in the exchange rate models as the resulting of nonlinearity, our model is able to produce endogenous exchange rate dynamics due to the presence of discontinuity induced by a sentiment index, which affects the way investors take their trading decisions. In particular, it affects the level of optimism/pessimism of fundamentalists regarding their perception on the value of fundamental. Moreover, it also affects the strength to which one kind of chartists places her buying/selling orders. We show that our model, represented by a two-dimensional discontinuous map, has the ability to produce interesting endogenous exchange rate dynamics. In addition, when each component of the map is buffeted by a stochastic component, the model closely replicates the stylized facts of the EUR/USD and EUR/JPY exchange rate markets.

1 Introduction

Economists have always paid close attention to the foreign exchange market. Furthermore, many researchers have highlighted that there is still much room for improvement in the models proposed in order to fully understand the dynamics hidden by the foreign exchange market. In this regard, [1] investigate the consequences of the introduction of floating exchange rates. In particular, the authors find interesting endogenous exchange rate dynamics due to the central bank interventions. In addition, there is a large consensus in the literature that models focusing on the rational expectations hypothesis are not able to match with empirical evidence of exchange rate markets. Instead, investors' decisions are influenced by psychological factors leading to the emergence of different beliefs about the behaviour of the exchange rate. This is the approach adopted, for example, by [1–10].

In line with the aforementioned literature, the aim of this paper is to analyse an exchange rate model with heterogeneous investors. In particular, we consider one kind of fundamentalists and two kinds of chartists. The introduction of these kinds of investors in the model is motivated by previous studies finding that the most part of heterogeneity in the market is due to the interaction between fundamentalists and chartists (see for example [6]). While fundamentalists believe in mean reversion of the exchange rate to its fundamental value, chartists believe in the persistence of the trend of the exchange rate and they place buying (selling) orders according to this trend being positive (negative).

Our model is characterized by the presence of two kinds of chartists. Chartists of kind 1 trade based upon the misalignment of the exchange rate to its fundamental value. In this respect, if the exchange rate is higher (lower) than its fundamental value chartists place buying (selling) orders. On the other hand, chartists of kind 2 derive their trading strategies from past exchange rate movements. In particular, chartists of kind 2 compare the current value of the exchange rate with its previous value in order to extrapolate the trend. Moreover, the rate at which these chartists extrapolate depends on a sentiment index inspired by that of [5]. According to this sentiment index, chartists of kind 2 are able to consider two trading signals. The first trading signal concerns the misalignment of the current exchange rate with respect to its previous value, which determines if chartists buy (if the misalignment is positive) or sell (if the misalignment is negative). The second trading signal refers to the strength of their activity. To this purpose, if the trend is positive, the amount of their buying orders depends on the distance between the current value of the exchange rate and its fundamental value. The introduction of the sentiment index in our model is consistent with the strand of literature confirming the importance of investor sentiment in affecting financial markets (see, e.g., [11]). In addition, we let the excess demand of fundamentalists to be positive or negative, even if there is no misalignment, in line with the evidence that there is no consensus on the exact value of the fundamental (see, for example, [8, 11–13]).

With the setup described above, the exchange rate evolution is defined by a two-dimensional discontinuous map with sets of discontinuity being represented by three border lines. Nonsmooth, in particular discontinuous, maps are known to display richer dynamics than the smooth ones due to existence of switching manifolds separating the state space into the regions in which the map is defined differently. When a point of an invariant set collides with such a manifold, a border collision bifurcation (BCB) may occur, which causes an abrupt change in the configuration of the invariant set (see, e.g., [14–17]).

For the map studied in the current work, BCB curves form main bifurcation structures observed in the parameter space. Below we will describe three such bifurcation structures. The first one is related to the infinite number of BCB curves issuing from a single point. It happens due to a *continuity breaking bifurcation* (see [18–20]), when a single fixed point may bifurcate to a cycle of any period as two parameters of the map change. Such two-parametric bifurcations are also referred to as *big bang bifurcations* ([21–24]) and were initially reported in one-dimensional nonsmooth maps. For the considered map, in the sufficiently close neighborhood of the big bang bifurcation point, the respective parameter plane is organized according to the period adding structure. Namely, the regions associated with cycles of different periods are ordered following the Farey summation rule, which is applied to the rotation numbers of the related cycles ([18, 25–27]).

Other period adding bifurcation structures (infinite in number) are observed when a parameter point moves away from the big bang bifurcation point. Each such structure is located between two disjoint periodicity regions related to cycles having the same period but associated with symbolic sequences that differ by one letter. Two neighbor regions belonging to two different period adding structures may overlap or may be disjoint. In the latter case, between these two regions there exists another period adding structure.

The third particular patchwork-like bifurcation structure is located between two regions related to cycles of period two and is related to cycles of even periods. We demonstrate that some of the periodicity regions belonging to this structure are organized according to the period adding principle, while ordering of the others correspond to the period incrementing principle, related to cycles with periods that form an arithmetic series.

Finally, we consider a stochastic version of the model in order to show that our model is able to replicate a broad list of features of typical time series behaviour. In particular, we will focus on a number of important stylized facts of the foreign exchange market, such as bubbles and crashes, fat-tailed return distributions and volatility clustering. This analysis is important for two main reasons. First, the parameter set used in the stochastic model is calibrated using the results of the deterministic skeleton. In this sense, the stochastic model serves as a robustness analysis of the deterministic part. Second, demonstrating the ability of our model to mimic the most important stylized fact of the foreign exchange market gives a great credibility to our approach.

The remainder of the paper is organized as follows. In Section 2, we present our behavioral exchange rate model. In Sections 3 and 4, we study the equilibrium properties and the resulting bifurcation structures of the model. Section 5 outlines the ability of our model to match the stylized facts of the EUR/USD and EUR/JPY exchange rate markets. Section 6 provides some concluding remarks.

2 The model

We develop a simple model of exchange rate determination where the market is populated by investors characterized by heterogeneous expectations. In particular, we assume the presence of three types of traders: one kind of fundamentalists and two kinds of chartists.

Before introducing the three types of traders, let us talk about the exchange rate formation mechanism. We assume existence of a market maker who collects all individual orders from traders and adjusts the exchange rate by looking at the excess demand, through the following rule:

$$S_{t+1} = S_t + \alpha \left(D_t^f + D_t^{c1} + D_t^{c2} \right), \tag{1}$$

where S denotes the log exchange rate, α is the nonnegative reaction parameter of the market maker, and D^f, D^{c1} and D^{c2} are the excess demands of fundamentalists, chartists of kind 1 and chartists of kind 2, respectively. If buying orders are more than selling orders, the market maker increases the exchange rate (and vice versa).

We assume that fundamentalists and chartists of kind 1 react asymmetrically when the asset is undervalued or overvalued. This assumption, adopted also by [28, 29], is coherent with some psychological theories of humans' decision making, like Prospect Theory [30], which emphasize the asymmetry of the human behavior when people face potential gains or potential losses.

The excess demand of fundamentalists is the following:

$$D_t^f = \begin{cases} f_a(F - S_t) - f_c & \text{if} \quad S_t - F > 0, \\ f_b(F - S_t) + f_d & \text{if} \quad S_t - F \leq 0, \end{cases} \tag{2}$$

where the nonnegative parameters f_a and f_b capture the reactivity of fundamentalists to the misalignment between the current value of the exchange rate and its fundamenal value (F), when it is overvalued and undervalued, respectively. Parameters $f_c \geq 0$ and $f_d \geq 0$ represent some kind of optimism/pessimism of fundamentalists when there is no misalignment.

Chartists of kind 1 are characterized by this piecewise-defined excess demand function:

$$D_t^{c1} = \begin{cases} c_a(S_t - F) & \text{if} \quad S_t - F > 0, \\ c_b(S_t - F) & \text{if} \quad S_t - F \leq 0, \end{cases} \tag{3}$$

where $c_a \geq 0$ and $c_b \geq 0$ are the different reactivities when the exchange rate is higher or lower than the fundamental value, respectively.

We additionally introduce a second kind of chartists, believing that there is something to learn also from the recent dynamics of the exchange rate itself. In particular, following [5], we let this kind of chartists extrapolate at a rate which depends on the magnitude of the misalignment. So, they operate by using the following trading rule:

$$D_t^{c2} = d_t r_t, \tag{4}$$

where $r_t := S_t - S_{t-1}$ is the one period exchange rate return, while d_t is time-varying sentiment coefficient. If it is positive, these traders are bandwagon and believe in the persistence of the trend, while if it is negative, they believe in a trend reversal. This sentiment coefficient depends on the absolute value of the misalignment and may switch between two regimes crossing a threshold value k_c of the absolute exchange rate return:

$$d_t = \begin{cases} d_1 \left| F - S_t \right| & \text{if} \quad |r_t| > k_c, \\ d_2 \left| F - S_t \right| & \text{if} \quad |r_t| \leq k_c. \end{cases} \tag{5}$$

In this work we only consider positive values of d_1 and d_2, characterizing a sort of bandwagon expectations of chartists. It seems more reasonable that chartists more strongly believe in the persistence of the trend when the misaligment is large. From now on we will fix $d_1 = 0.2$ and $d_2 = 0.1$. We leave the study of the other cases for future works.

By putting all the excess demands into the market maker equation (1), we get the following dynamical system regulating the dynamics of the exchange rate:

$$S_{t+1} = \begin{cases} S_t + \left[-f_a \Delta S_t - f_c + c_a \Delta S_t + d_1 \Delta S_t \left(S_t - S_{t-1}\right)\right] & \text{if} \quad \Delta S_t > 0 \wedge |S_t - S_{t-1}| > k_c, \\ S_t + \left[-f_a \Delta S_t - f_c + c_a \Delta S_t + d_2 \Delta S_t \left(S_t - S_{t-1}\right)\right] & \text{if} \quad \Delta S_t > 0 \wedge |S_t - S_{t-1}| \leq k_c, \\ S_t + \left[-f_b \Delta S_t + f_d + c_b \Delta S_t + d_1 \Delta S_t \left(S_t - S_{t-1}\right)\right] & \text{if} \quad \Delta S_t \leq 0 \wedge |S_t - S_{t-1}| > k_c, \\ S_t + \left[-f_b \Delta S_t + f_d + c_b \Delta S_t + d_2 \Delta S_t \left(S_t - S_{t-1}\right)\right] & \text{if} \quad \Delta S_t \leq 0 \wedge |S_t - S_{t-1}| \leq k_c \end{cases} \tag{6}$$

with $\Delta S_t = S_t - F$.

We can simplify the notation by introducing the auxiliary variable $X = S - F$, which measures the misalignment. The dynamical system (6) is made up of the second-order difference equations and it can be reconducted to a two-dimensional system of difference equations by introducing the lagged variable $Y_{t+1} = X_t$. In such a way, we get the two-dimensional map $T : (X, Y) \mapsto$

(X', Y') with

$$X' = f(X,Y) := \begin{cases} X + c_a X - f_a X - f_c + d_1 X(X-Y) & \text{if} \;\; X > 0 \wedge |X-Y| > k_c, \\ X + c_a X - f_a X - f_c + d_2 X(X-Y) & \text{if} \;\; X > 0 \wedge |X-Y| \leq k_c, \\ X + c_b X - f_b X + f_d - d_1 X(X-Y) & \text{if} \;\; X \leq 0 \wedge |X-Y| > k_c, \\ X + c_b X - f_b X + f_d - d_2 X(X-Y) & \text{if} \;\; X \leq 0 \wedge |X-Y| \leq k_c, \end{cases} \tag{7a}$$

$$Y' = X, \tag{7b}$$

where the symbol "$'$" denotes the unit-time advancement operator.

3 Preliminary analysis

First, let us introduce new auxiliary parameters

$$a = 1 + c_a - f_a, \quad b = 1 + c_b - f_b. \tag{8}$$

Then function (7a) acquires the form

$$f(X,Y) = \begin{cases} f_1(X,Y) := d_1 X^2 - d_1 XY + aX - f_c & \text{if} \;\; X > 0 \wedge |X-Y| > k_c, \\ f_2(X,Y) := d_2 X^2 - d_2 XY + aX - f_c & \text{if} \;\; X > 0 \wedge |X-Y| \leq k_c, \\ f_3(X,Y) := -d_1 X^2 + d_1 XY + bX + f_d & \text{if} \;\; X \leq 0 \wedge |X-Y| > k_c, \\ f_4(X,Y) := -d_2 X^2 + d_2 XY + bX + f_d & \text{if} \;\; X \leq 0 \wedge |X-Y| \leq k_c. \end{cases} \tag{9}$$

Second, through the homeomorphism

$$h(X,Y) = (k_c X, k_c Y), \tag{10}$$

the map T with f as defined in (9) is topologically conjugate to the map $\tilde{T}$ with

$$\tilde{f}(X,Y) = \begin{cases} \tilde{f}_1(X,Y) = \tilde{d}_1 X^2 - \tilde{d}_1 XY + aX - \tilde{f}_c & \text{if} \;\; X > 0 \wedge |X-Y| > 1, \\ \tilde{f}_2(X,Y) = \tilde{d}_2 X^2 - \tilde{d}_2 XY + aX - \tilde{f}_c & \text{if} \;\; X > 0 \wedge |X-Y| \leq 1, \\ \tilde{f}_3(X,Y) = -\tilde{d}_1 X^2 + \tilde{d}_1 XY + bX + \tilde{f}_d & \text{if} \;\; X \leq 0 \wedge |X-Y| > 1, \\ \tilde{f}_4(X,Y) = -\tilde{d}_2 X^2 + \tilde{d}_2 XY + bX + \tilde{f}_d & \text{if} \;\; X \leq 0 \wedge |X-Y| \leq 1, \end{cases} \tag{11}$$

where

$$\tilde{d}_i = d_i k_c, \; i = 1, 2, \quad \tilde{f}_i = \frac{f_i}{k_c}, \; i = c, d. \tag{12}$$

Hence, for analysing qualitative dynamics of the map T with f defined in (9) and the second equation given by (7b), one can fix $k_c = 1$ without losing generality. So we do everywhere below.

The map T is discontinuous and its switching manifolds (the sets of discontinuity) are represented by three border lines

$$B_{\pm} = \{(X, Y) \,:\, Y = X \pm 1\} \quad \text{and} \quad B_0 = \{(X, Y) \,:\, X = 0\}, \tag{13}$$

which divide the state space into six regions of definition:

$$\begin{aligned}
&\mathcal{D}_{\mathcal{R}_-} = \{(X, Y) \,:\, X > 0, Y < X - 1\}, \quad \mathcal{D}_{\mathcal{R}_+} = \{(X, Y) \,:\, X > 0, Y > X + 1\},\\
&\mathcal{D}_{\mathcal{R}_0} = \{(X, Y) \,:\, X > 0, X - 1 \le Y \le X + 1\},\\
&\mathcal{D}_{\mathcal{L}_-} = \{(X, Y) \,:\, X \le 0, Y < X - 1\}, \quad \mathcal{D}_{\mathcal{L}_+} = \{(X, Y) \,:\, X \le 0, Y > X + 1\},\\
&\mathcal{D}_{\mathcal{L}_0} = \{(X, Y) \,:\, X \le 0, X - 1 \le Y \le X + 1\}.
\end{aligned} \tag{14}$$

The function f_1 is applied in the regions $\mathcal{D}_{\mathcal{R}_-}$ and $\mathcal{D}_{\mathcal{R}_+}$, the function f_3 in the regions $\mathcal{D}_{\mathcal{L}_-}$ and $\mathcal{D}_{\mathcal{L}_+}$, the function f_2 in the region $\mathcal{D}_{\mathcal{R}_0}$, while the function f_4 in the region $\mathcal{D}_{\mathcal{L}_0}$. In Fig. 1 we plot the state space filling in the regions of definition $\mathcal{D}_s$, $s \in \{\mathcal{L}_-, \mathcal{L}_0, \mathcal{L}_+, \mathcal{R}_-, \mathcal{R}_0, \mathcal{R}_+\}$ by different colors.

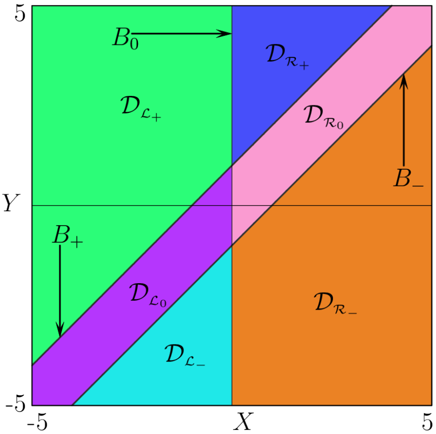

Fig. 1 Regions of definition $\mathcal{D}_s$, $s \in \{\mathcal{L}_-, \mathcal{L}_0, \mathcal{L}_+, \mathcal{R}_-, \mathcal{R}_0, \mathcal{R}_+\}$.

As it is often done for piecewise smooth systems, every point (X, Y) in the state space is associated with a respective symbol, depending on the region of definition $\mathcal{D}_s$, $s \in \{\mathcal{L}_-, \mathcal{L}_0, \mathcal{L}_+, \mathcal{R}_-, \mathcal{R}_0, \mathcal{R}_+\}$ the point belongs to. In such a way, any orbit $\tau = \{(X_0, Y_0), (X_1, Y_1), \ldots, (X_i, Y_i), \ldots\}$ of the map T has correspondence with a symbolic sequence $\sigma(\tau) = s_0 s_1 \ldots s_i \ldots$ with s_i such that $(X_i, Y_i) \in \mathcal{D}_{s_i}$. Note that due to the second component of the map T, the sequence of Y_i values, except for the initial Y_0, is represented by the sequence of X_i's shifted by one.

If the orbit τ is periodic (a cycle) of period n, its symbolic sequence is clearly finite (consisting of n symbols). In such a case we use the notation $\mathcal{O}_\sigma := \{p_1, p_2, \ldots, p_n\}$, where $p_i = (X_i, Y_i)$, $i = 1, \ldots, n$ and $\sigma = s_1 s_2 \ldots s_n$ with the sequence σ being shift invariant. Clearly, for $\mathcal{O}_\sigma$ there is $Y_i = X_{i-1}$, $i = 2, \dots, n$ and $Y_1 = X_n$, that is, $\mathcal{O}_\sigma = \{(X_1, X_n), (X_2, X_1), \dots, (X_n, X_{n-1})\}$. Hence, every n-cycle is defined by n values of the first coordinate, while the values of the second coordinate consist of the same sequence of numbers shifted by one. This property restricts location of cycles in the state space (in particular, 2-cycles are always symmetric with respect to the main diagonal $Y = X$).

Each point p_i of the cycle $\mathcal{O}_\sigma$ is related to a particular cyclical permutation of σ, namely, if p_1 corresponds to $s_1 \dots s_n$ then p_2 corresponds to $s_2 \dots s_n s_1$, p_3 to $s_3 \dots s_n s_1 s_2$, and so on. Whenever it is necessary to distinguish different points of the cycle (for instance, to provide an explicit condition at a border collision), we use the notation $p_i := p_{s_i s_{i+1} \dots s_n \dots s_{i-1}} = (X_i, X_{i-1})$ with $X_i = X_{s_i s_{i+1} \dots s_n \dots s_{i-1}}$. For example, let us consider a cycle $\mathcal{O}_{\mathcal{L}_+ \mathcal{L}_0 \mathcal{R}_0} = \{p_1, p_2, p_3\}$, then $p_1 = (X_1, X_3) := p_{\mathcal{L}_+ \mathcal{L}_0 \mathcal{R}_0}$, $p_2 = (X_2, X_1) := p_{\mathcal{L}_0 \mathcal{R}_0 \mathcal{L}_+}$, $p_3 = (X_3, X_2) := p_{\mathcal{R}_0 \mathcal{L}_+ \mathcal{L}_0}$, where correspondingly $X_1 = X_{\mathcal{L}_+ \mathcal{L}_0 \mathcal{R}_0}$, $X_2 = X_{\mathcal{L}_0 \mathcal{R}_0 \mathcal{L}_+}$, and $X_3 = X_{\mathcal{R}_0 \mathcal{L}_+ \mathcal{L}_0}$.

In the prameter space, a region associated with a cycle $\mathcal{O}_\sigma$ is called the *periodicity region* and is denoted as $\mathcal{P}_\sigma$.[1]

3.1 Fixed points and their stability

From the second component of the map T, it is clear that the fixed points of T must belong to the diagonal $Y = X$. This implies that the functions f_1 and f_3 can be related to virtual fixed points only. Let us find fixed points defined by using f_2 and f_4, that is, those which belong to the regions $\mathcal{D}_{\mathcal{R}_0}$ and $\mathcal{D}_{\mathcal{L}_0}$, respectively. One obtains two fixed points $E_{\mathcal{L}_0} = (X^*_{\mathcal{L}_0}, X^*_{\mathcal{L}_0}) \in \mathcal{D}_{\mathcal{L}_0}$ by using f_4 and $E_{\mathcal{R}_0} = (X^*_{\mathcal{R}_0}, X^*_{\mathcal{R}_0}) \in \mathcal{D}_{\mathcal{R}_0}$ by using f_2 with

$$X^*_{\mathcal{L}_0} = -\frac{f_d}{b-1}, \quad X^*_{\mathcal{R}_0} = \frac{f_c}{a-1}. \tag{15}$$

If $a < 1$ (i.e., $c_a < f_a$), the point $E_{\mathcal{R}_0}$ is virtual, and if $b < 1$ (i.e., $c_b < f_b$), the point $E_{\mathcal{L}_0}$ is virtual.

To investigate the stability of the fixed points of the map T defined by (9) and (7b), we have to compute the Jacobian matrix. Since the map is nonsmooth, there are four such matrices, according to the functions f_i, $i = 1, \dots, 4$, acting in the respective regions of definition:

$$J_1(X,Y) = \begin{pmatrix} 2d_1X - d_1Y + a & -d_1X \\ 1 & 0 \end{pmatrix}, \quad J_2(X,Y) = \begin{pmatrix} 2d_2X - d_2Y + a & -d_2X \\ 1 & 0 \end{pmatrix},$$
$$J_3(X,Y) = \begin{pmatrix} -2d_1X + d_1Y + b & d_1X \\ 1 & 0 \end{pmatrix}, \quad J_4(X,Y) = \begin{pmatrix} -2d_2X + d_2Y + b & d_2X \\ 1 & 0 \end{pmatrix}. \tag{16}$$

[1] If the cycle is attracting, one can discover the respective periodicity region by numerical simulation. However, if the cycle is repelling (or a saddle), the periodicity region is not observable numerically, though it exists.

For the point $E_{\mathcal{L}_0}$, the Jacobian matrix is

$$J_4(X^*_{\mathcal{L}_0}, X^*_{\mathcal{L}_0}) := J^*_{\mathcal{L}_0} = \begin{pmatrix} \frac{f_d d_2}{b-1} + b & -\frac{f_d d_2}{b-1} \\ 1 & 0 \end{pmatrix}. \tag{17}$$

Then

$$\mathrm{tr} J^*_{\mathcal{L}_0} = \frac{f_d d_2}{b-1} + b, \quad \det J^*_{\mathcal{L}_0} = \frac{f_d d_2}{b-1}, \tag{18}$$

and the Jury conditions [31, 32], read as

$$1 - \mathrm{tr} J^*_{\mathcal{L}_0} + \det J^*_{\mathcal{L}_0} = 1 - b > 0, \tag{19a}$$

$$1 + \mathrm{tr} J^*_{\mathcal{L}_0} + \det J^*_{\mathcal{L}_0} = 1 + \frac{2 f_d d_2}{b-1} + b > 0, \tag{19b}$$

$$\det J^*_{\mathcal{L}_0} = \frac{f_d d_2}{b-1} < 1. \tag{19c}$$

When $E_{\mathcal{L}_0}$ is not virtual (that is, $X^*_{\mathcal{L}_0} < 0$, and hence, $b > 1$), condition (19a) does not hold, and $E_{\mathcal{L}_0}$ can not be stable. If additionally condition (19b) does not hold, $E_{\mathcal{L}_0}$ is an unstable node. Otherwise, $E_{\mathcal{L}_0}$ is a saddle.

Similary for the point $E_{\mathcal{R}_0}$, the Jacobian matrix is

$$J_2(X^*_{\mathcal{R}_0}, X^*_{\mathcal{R}_0}) := J^*_{\mathcal{R}_0} = \begin{pmatrix} \frac{f_c d_2}{a-1} + a & -\frac{f_c d_2}{a-1} \\ 1 & 0 \end{pmatrix}. \tag{20}$$

Then

$$\mathrm{tr} J^*_{\mathcal{R}_0} = \frac{f_c d_2}{a-1} + a, \quad \det J^*_{\mathcal{R}_0} = \frac{f_c d_2}{a-1}, \tag{21}$$

and the Jury conditions read as

$$1 - \mathrm{tr} J^*_{\mathcal{R}_0} + \det J^*_{\mathcal{R}_0} = 1 - a > 0, \tag{22a}$$

$$1 + \mathrm{tr} J^*_{\mathcal{R}_0} + \det J^*_{\mathcal{R}_0} = 1 + \frac{2 f_c d_2}{a-1} + a > 0, \tag{22b}$$

$$\det J^*_{\mathcal{R}_0} = \frac{f_c d_2}{a-1} < 1. \tag{22c}$$

When $E_{\mathcal{R}_0}$ is not virtual (that is, $X^*_{\mathcal{R}_0} > 0$, and hence, $a > 1$), condition (22a) does not hold, and $E_{\mathcal{R}_0}$ can not be stable. If additionally condition (22b) does not hold, $E_{\mathcal{R}_0}$ is an unstable node. Otherwise, $E_{\mathcal{R}_0}$ is a saddle.

3.2 Critical set

As we have shown above, the map T cannot have any (nonvirtual) stable fixed points. In order to study asymptotic dynamics of T further, we should recall the notion of a *critical set*, which plays an important role when one describes qualitative changes of invariant sets and their basins of attraction. For continuous maps, critical sets are the analogues of the sets of local extrema values for smooth one-dimensional noninvertible maps, and the set having the first derivative equal to zero is replaced by the set at which the Jacobian determinant is equal to zero (see, e.g., [33–36]). For continuous piecewise smooth maps, a *critical set* LC is defined as a geometric locus of points in the phase space having at least two coincident preimages. These coincident preimages are located on the set LC_{-1} including the switching manifolds, as well as the set of points at which the Jacobian determinant vanishes. The significance of the critical set follows from the fact that its branches separate the state space into regions containing points with different number of first rank preimages. Further images of the critical set, referred to as critical sets of higher ranks, are also used to obtain the boundaries of trapping areas and to study transformations of basins of attraction.

For maps defined by discontinuous functions, the set LC_{-1} is defined in the same way as for continuous piecewise smooth maps, that is, it consists of both—the set of vanishing Jacobian determinant, in case it exists, and the switching manifolds (including the points of discontinuity). However, the definition of the critical set LC is slightly modified. Namely, for each switching manifold given by the points of discontinuity, one obtains two first rank images by using different determinations of the map at both sides of this switching manifold. Then these two images belong to the critical set LC if they represent boundaries of the regions containing points with different number of first rank preimages (see, e.g., [34]).

For the map T, the condition $\det J_i(X,Y) = 0$, $i = 1,\ldots,4$ holds for $X = 0$ with J_i defined in (16). Hence, the set LC_{-1} is only made up of the points of discontinuity. For every point $(0,Y) \in B_0$, $Y \in \mathbb{R}$, we compute two different images by using the functions f_2 and f_4 (if $|Y| \leq 1$) or f_1 and f_3 (if $|Y| > 1$). Since

$$f_1(0,Y) = f_2(0,Y) = -f_c,$$
$$f_3(0,Y) = f_4(0,Y) = f_d,$$

the image of the border line B_0 is represented by two points, $(-f_c, 0)$ and $(f_d, 0)$. The images of the other two border lines $B_\pm$ by using f_i, $i = 1,\ldots,4$ are given by the following eight lines, respectively:

$$\begin{aligned}
B_{1,\pm} &= \left\{(X,Y)\,:\,Y = \frac{X+f_c}{a \mp d_1}, Y > 0\right\},\\
B_{2,\pm} &= \left\{(X,Y)\,:\,Y = \frac{X+f_c}{a \mp d_2}, Y > 0\right\},\\
B_{3,\pm} &= \left\{(X,Y)\,:\,Y = \frac{X-f_d}{b \pm d_1}, Y \leq 0\right\},\\
B_{4,\pm} &= \left\{(X,Y)\,:\,Y = \frac{X-f_d}{b \pm d_2}, Y \leq 0\right\}.
\end{aligned} \tag{23}$$

The lines $B_{i,\pm}$, $i = 1, \ldots, 4$ confine images of the regions $\mathcal{D}_s$, $s \in \{\mathcal{L}_-, \mathcal{L}_0, \mathcal{L}_+, \mathcal{R}_-, \mathcal{R}_0, \mathcal{R}_+\}$.

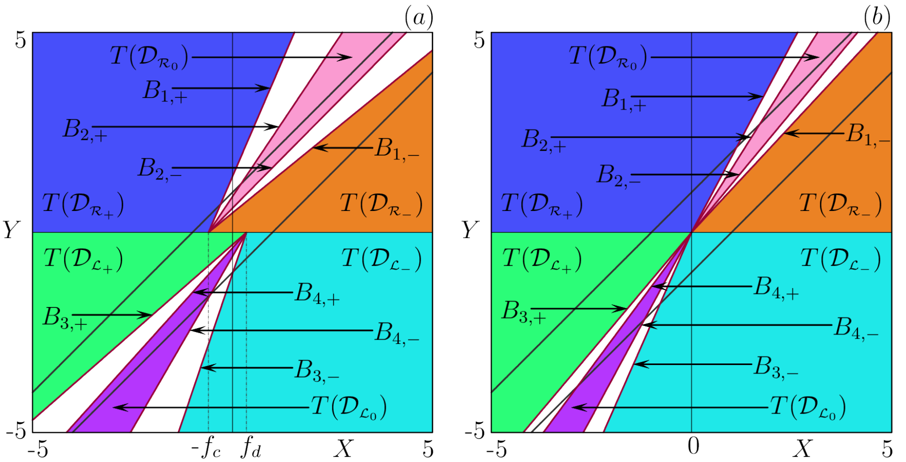

Fig. 2 (a) Typical view of the images of the regions $\mathcal{D}_s$ in the case $d_1 > d_2$, filled in with the same colors as $\mathcal{D}_s$ in Fig. 1. (b) Particular case of (a) with $f_c = f_d = 0$.

In Fig. 2(a) we plot images of $\mathcal{D}_s$ for the case $d_1 > d_2$ using the same respective colors. Note that each $T(\mathcal{D}_s)$ is a part of the Z_1 region (each point has exactly one first rank preimage), while white color corresponds to Z_0 region (each point has no preimages), and hence, the map is invertible. On the contrary, for $d_1 < d_2$, the map T is noninvertible but here we focus on the invertible case, keeping more sophisticated studies for future work. The panel (b) of the same figure shows $T(\mathcal{D}_s)$ for $d_1 > d_2$ and $f_c = f_d = 0$, a particular parameter constellation which will be considered below.

It is worth noting that the horizontal axis $Y = 0$ also serves as a border between $T(\mathcal{D}_{\mathcal{L}_+})$, $T(\mathcal{D}_{\mathcal{R}_+})$, $T(\mathcal{D}_{\mathcal{L}_-})$ and $T(\mathcal{D}_{\mathcal{R}_-})$, although this line is not an image of any of the switching manifolds. To explain this issue, let us take a sample point $(X', \varepsilon) \in T(\mathcal{D}_{\mathcal{R}_+})$ with some fixed $X' < -f_c$ and $0 < \varepsilon \ll 1$. Its preimage (X, Y) is obtained by using the function f_1 for the first coordinate, from where we have $X = \varepsilon$ and

$$X' = d_1\varepsilon^2 - d_1\varepsilon Y + a\varepsilon - f_c \quad \Leftrightarrow \quad Y = \varepsilon + \frac{a}{d_1} - \frac{f_c + X'}{d_1\varepsilon}. \tag{24}$$

Clearly, the smaller ε and/or the larger the absolute value of X', the larger Y. More precisely,

$$\lim_{\varepsilon \to 0} \left(\varepsilon + \frac{a}{d_1} - \frac{f_c + X'}{d_1\varepsilon} \right) = +\infty \quad \text{and} \quad \lim_{X' \to -\infty} \left(\varepsilon + \frac{a}{d_1} - \frac{f_c + X'}{d_1\varepsilon} \right) = +\infty. \tag{25}$$

Roughy speaking, the image of the switching manifold B_0 (for a bounded value of Y) under T with f_1 is contracted to the point $(-f_c, 0)$, while the limit point $(0, +\infty)$ is unfolded into the ray $\{(X', Y') : X' < -f_c, Y' = 0\}$. Likewise, the limit point $(0, -\infty)$ is unfolded by using f_1 into the ray $\{(X', Y') : X' > -f_c, Y' = 0\}$. For the images $T(\mathcal{D}_{\mathcal{L}_+})$ and $T(\mathcal{D}_{\mathcal{L}_-})$ one can apply a similar argument but by using f_3 instead of f_1 and f_d instead of $-f_c$.

4 Bifurcation structures in the parameter space

In what follows we describe some typical bifurcation structures uncovered in the parameter space of the map T. In Fig. 3 we plot two typical 2D bifurcation diagrams in (f_c, f_d) parameter plane for a fixed $0 < b < 1$, one with $0 < a < 1$ and the other with $a > 1$, where regions of distinct colors correspond to attracting cycles of different periods.

As the first observation, we notice a bunch of regions issuing from the single point $(f_c, f_d) = (0, 0)$ and related to attracting cycles with symbolic sequences having only letters $\mathcal{L}_0$ and $\mathcal{R}_0$. Similar bifurcation structures are also detected in a neighborhood of a specific type of organizing centers (bifurcation points of codimension two) in the parameter space, commonly called *big bang bifurcations* ([21–23]). Bifurcations of this type are characterized by the infinite number of bifurcation curves issuing from a single point and were initially reported in one-dimensional piecewise smooth maps, although they are known to occur in maps of higher dimensions as well. In particular, a big bang bifurcation may occur in a 1D map due to the phenomenon known as *continuity breaking* ([18–20]). In such a case, a single fixed point existing for the continuous version of a map may bifurcate to a cycle of any period when the continuity is destroyed.

For larger values of f_c and f_d, there are periodicity regions for cycles having symbolic sequences that involve also the other two symbols $\mathcal{L}_+$ and $\mathcal{R}_-$. In most cases, two neighbor regions related to the same base period (say, n) are associated with symbolic sequences that differ for one letter. For $a = 1.15$ (see Fig. 3(b)), these neighbor regions often overlap leading to coexistence of the two cycles of the same period (see, e.g., the right-hand side inset related to period three). On the contrary, for $a = 0.73$ (see Fig. 3(a)), neighbor regions corresponding to the same period n are usually separated from each other by another bifurcation structure. The latter is related to periods that are factors of the base period (namely, $j \cdot n$, $j = 2, 3, \ldots$; see the insets in panel (a)). Note that for $n = 2$, this structure is particular as will be shown below.

4.1 Continuity breaking: Period adding on symbols $\mathcal{L}_0$ and $\mathcal{R}_0$

Let us consider a particular case of $f_c = f_d = 0$. Then, the map T is continuous at the switching manifold B_0; however, it is still discontinuous at the other two border lines $B_\pm$. The images $T(\mathcal{D}_{\mathcal{L}_0})$ and $T(\mathcal{D}_{\mathcal{R}_0})$ issue from the origin $(0, 0)$ (see Fig. 2(b)), which is now a fixed point, since $E_{\mathcal{L}_0} = E_{\mathcal{R}_0} = (0, 0)$. The point

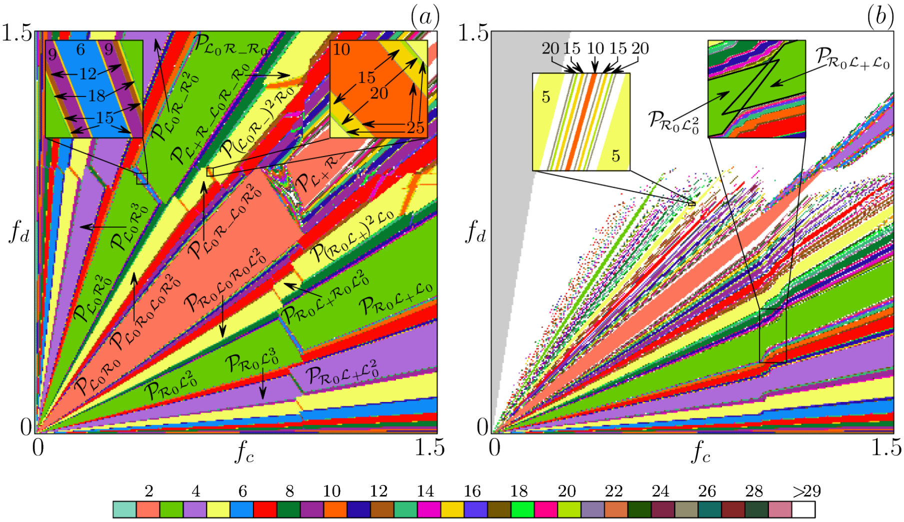

Fig. 3 Typical 2D BD in (f_c, f_d) parameter plane for $b = 0.64, d_1 = 0.2, d_2 = 0.1$ and (a) $a = 0.73$; (b) $a = 1.15$.

$(0, 0)$ has two different Jacobian matrices, the right and the left, respectively:

$$J_{\mathcal{L}_0}(0,0) = \begin{pmatrix} a & 0 \\ 1 & 0 \end{pmatrix} \quad \text{and} \quad J_{\mathcal{R}_0}(0,0) = \begin{pmatrix} b & 0 \\ 1 & 0 \end{pmatrix}. \tag{26}$$

Clearly, the stability of $(0, 0)$ depends on the values of a and b, because the second multiplier is always zero. Thus, if $|a| < 1$ ($|b| < 1$) the point is stable from the right-hand (left-hand) side. If both $|a| > 1$, $|b| > 1$, the origin is a saddle being always superstable along $Y = 0$ (in the vertical direction).

If at least one of the two parameters f_c or f_d becomes different from zero, the discontinuity of T at B_0 is restored, leading to a continuity breaking bifurcation. Let us fix a parameter pair (f_c, f_d) such that f_c and f_d are positive but sufficiently close to zero. Orbits that are close to the origin can be approximated by considering the linearization of the map T in the neighborhood of $(0, 0)$, given by $DT|_{(0,0)}\colon \mathbb{R}^2 \ni (X, Y) \to (X', Y') \in \mathbb{R}^2$ with

$$X' = g(X) = \begin{cases} aX - f_c & \text{if} \quad X > 0, \\ bX + f_d & \text{if} \quad X \leq 0 \end{cases} \tag{27}$$

and $Y' = X$. As one can see, the first component does not depend on Y, as well as the second one. Therefore, locally for (f_c, f_d) close to $(0, 0)$, asymptotic dynamics of T in the neighborhood of the origin can be approximated by a one-dimensional piecewise linear map g defined in two partitions of the increasing-increasing type with a positive jump. In the parameter plane (f_c, f_d) of the map g the point $(0, 0)$ is a point of the big bang bifurcation. Periodicity regions issuing from this point and related to attracting cycles of different

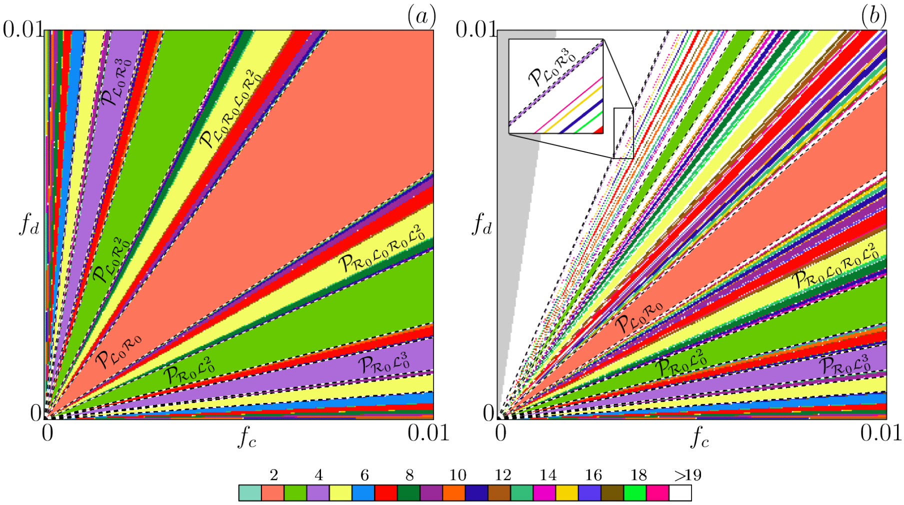

Fig. 4 2D BD in (f_c, f_d) parameter plane in the neighborhood of the continuity breaking bifurcation point with $b = 0.64, d_1 = 0.2, d_2 = 0.1$ and (a) $a = 0.73$; (b) $a = 1.15$.

periods are organized in a period adding bifurcation structure, fully described in, e.g., [37, 38] (see also [39] and references therein). These periodicity regions are ordered in the parameter space according to Farey summation rule, applied to the rotation numbers of the corresponding cycles. Namely, between two disjoint periodicity regions $\mathcal{P}_{\sigma_1}$ and $\mathcal{P}_{\sigma_2}$ related to cycles $\mathcal{O}_{\sigma_1}$ and $\mathcal{O}_{\sigma_2}$, respectively, whose rotation numbers $\frac{q_1}{n_1}$ and $\frac{q_2}{n_2}$ are Farey neighbors, there exists a periodicity region $\mathcal{P}_{\sigma_1\sigma_2}$ related to the cycle $\mathcal{O}_{\sigma_1\sigma_2}$ whose rotation number is $\frac{q_1+q_2}{n_1+n_2}$.

Such an ordering can be clearly distinguished also in Fig. 4 in the neighborhood of $(0, 0)$, for the cycles having symbolic sequences consisting of the letters $\mathcal{L}_0$ and $\mathcal{R}_0$. Indeed, in panel (a) with both $0 < a < 1$ and $0 < b < 1$, one observes the regions (of the so-called first complexity level) $\mathcal{P}_{\mathcal{L}_0{\mathcal{R}_0}^n}$ and $\mathcal{P}_{\mathcal{R}_0{\mathcal{L}_0}^n}$, $n = 1, 2, \ldots$ Between any two neighbor regions $\mathcal{P}_{\mathcal{L}_0{\mathcal{R}_0}^n}$ and $\mathcal{P}_{\mathcal{L}_0{\mathcal{R}_0}^{n+1}}$ there are regions $\mathcal{P}_{\mathcal{L}_0{\mathcal{R}_0}^n(\mathcal{L}_0{\mathcal{R}_0}^{n+1})^m}$ and $\mathcal{P}_{(\mathcal{L}_0{\mathcal{R}_0}^n)^m\mathcal{L}_0{\mathcal{R}_0}^{n+1}}$, $m = 1, 2, \ldots$ (of the so-called second complexity level), while between $\mathcal{P}_{\mathcal{R}_0{\mathcal{L}_0}^n}$ and $\mathcal{P}_{\mathcal{R}_0{\mathcal{L}_0}^{n+1}}$ there are sequences of $\mathcal{P}_{\mathcal{R}_0{\mathcal{L}_0}^n(\mathcal{R}_0{\mathcal{L}_0}^{n+1})^m}$ and $\mathcal{P}_{(\mathcal{R}_0{\mathcal{L}_0}^n)^m\mathcal{R}_0{\mathcal{L}_0}^{n+1}}$. And so on.

The boundaries of these regions, issuing from the point $(0, 0)$, are related to BCBs at which one of the cycle points collides with the border line B_0. More precisely, for the region $\mathcal{P}_{\mathcal{L}_0{\mathcal{R}_0}^n}$ its upper boundary is related to the condition $(X_{\mathcal{L}_0{\mathcal{R}_0}^n}, X_{\mathcal{R}_0\mathcal{L}_0{\mathcal{R}_0}^{n-1}}) \in B_0$ or, equivalently, $X_{\mathcal{L}_0{\mathcal{R}_0}^n} = 0$ (the same condition as for the 1D map g). As for its lower boundary, it is associated with the collision $(X_{\mathcal{R}_0\mathcal{L}_0{\mathcal{R}_0}^{n-1}}, X_{{\mathcal{R}_0}^2\mathcal{L}_0{\mathcal{R}_0}^{n-2}}) \in B_0$ or, equivalently, $X_{\mathcal{R}_0\mathcal{L}_0{\mathcal{R}_0}^{n-1}} = 0$. In Fig. 4, the dashed lines represent the analytically computed BCB boundaries (given by linear functions) for the linear 1D map g. As one can conclude, they provide a good approximation of the bifurcation boundaries for the 2D map T with f_c and f_d being sufficiently close to zero.

In Fig. 4(b) there is $a > 1$, and the group of regions related to symbolic sequences $\mathcal{L}_0\mathcal{R}_0^n$ is truncated at period four, i.e., at $\mathcal{P}_{\mathcal{L}_0{\mathcal{R}_0}^3}$. It happens due to that the cycles having more points in $\mathcal{D}_{\mathcal{R}_0}$ are not stable. Indeed, there is $ba^3 < 1$, while for $n > 3$ there is $ba^n > 1$. Hence, at the continuity breaking bifurcation, the cycles $\mathcal{O}_{\mathcal{L}_0{\mathcal{R}_0}^n}$ with $n > 3$ appear unstable.

4.2 Moving further from the big bang bifurcation

When f_c and f_d increase, the influence of the nonlinear terms in the expression for f_i, $i = 1, \ldots, 4$ becomes more significant and the aforementioned BCB boundaries of the regions forming the period adding structure become curved.[2] Additionally, the images $T(\mathcal{D}_{\mathcal{L}_0})$ and $T(\mathcal{D}_{\mathcal{R}_0})$ become more displaced from the origin (cf. Figs. 2(b) and (a)). This implies that the points of a cycle move towards one of the other two switching manifolds $B_\pm$, eventually crossing them one by one.

In Fig. 3 for larger values of f_c and f_d, one can see the periodicity regions associated with symbolic sequences having not only $\mathcal{L}_0$ and $\mathcal{R}_0$ but also $\mathcal{L}_+$ and $\mathcal{R}_-$. In most cases, symbolic sequences corresponding to two neighbor regions related to the same period differ for one letter. For example, the pairs $\mathcal{P}_{\mathcal{R}_0{\mathcal{L}_0}^2}$ and $\mathcal{P}_{\mathcal{R}_0\mathcal{L}_+\mathcal{L}_0}$, $\mathcal{P}_{\mathcal{L}_0{\mathcal{R}_0}^2}$ and $\mathcal{P}_{\mathcal{L}_0\mathcal{R}_-\mathcal{R}_0}$, $\mathcal{P}_{\mathcal{R}_0\mathcal{L}_0\mathcal{R}_0{\mathcal{L}_0}^2}$ and $\mathcal{P}_{\mathcal{R}_0\mathcal{L}_+\mathcal{R}_0{\mathcal{L}_0}^2}$, $\mathcal{P}_{\mathcal{R}_0\mathcal{L}_+\mathcal{R}_0{\mathcal{L}_0}^2}$ and $\mathcal{P}_{\mathcal{R}_0\mathcal{L}_+\mathcal{R}_0\mathcal{L}_+\mathcal{L}_0}$, and so forth. One of the exceptions are the regions related to period two, $\mathcal{P}_{\mathcal{L}_0\mathcal{R}_0}$ and $\mathcal{P}_{\mathcal{L}_+\mathcal{R}_-}$, considered in more detail in the next section.

Such a dependence of the symbolic sequences associated with neighbor regions can be easily explained. As shown above for (f_c, f_d) being sufficiently close to $(0, 0)$, points of cycles are located near the origin in the state space. If the parameter point (f_c, f_d) is moved away from $(0, 0)$ so that it always belongs to a particular region $\mathcal{P}_\sigma$, $\sigma = s_1 \ldots s_n$, $s_i \in \{\mathcal{L}_0, \mathcal{R}_0\}$, $i = 1, \ldots, n$, then some of the points of the respective cycle move towards one of the other two switching manifolds $B_\pm$. As a rule, only one point at a time collides with either B_+ or B_-. This leads to another BCB corresponding to the third boundary of $\mathcal{P}_\sigma$. Since the map T is discontinuous at $B_\pm$, the cycle of the same period having the symbolic sequence with one symbol changed cannot appear immediately after this BCB. Two regions $\mathcal{P}_\sigma$ and $\mathcal{P}_{\sigma'}$ related to the same period n, with σ and σ' being different for one letter, can be located with respect to each other in two ways: (i) they can be disjoint and separated from each other by a sequence of regions related to periods $j \cdot n$, $j = 2, 3, \ldots$ (as most of the region pairs in Fig. 3(a) for $a < 1$); (ii) they can overlap leading to coexistence of the two cycles (as the majority of regions in Fig. 3(b) for $a > 1$).

Let us consider a typical region $\mathcal{P}_{\mathcal{L}_0{\mathcal{R}_0}^2}$ for $a < 1$, from the period adding structure in the neighborhood of its third BCB boundary, far from the point $f_c = f_d = 0$ (see Fig. 5). The respective 3-cycle is

$$\mathcal{O}_{\mathcal{L}_0{\mathcal{R}_0}^2} = \{(X_{\mathcal{L}_0{\mathcal{R}_0}^2}, X_{\mathcal{R}_0\mathcal{L}_0\mathcal{R}_0}), (X_{{\mathcal{R}_0}^2\mathcal{L}_0}, X_{\mathcal{L}_0{\mathcal{R}_0}^2}), (X_{\mathcal{R}_0\mathcal{L}_0\mathcal{R}_0}, X_{{\mathcal{R}_0}^2\mathcal{L}_0})\}. \quad (28)$$

[2]It is possible to compute the analytic expressions of these boundaries for the cycles $\mathcal{O}_{\mathcal{L}_0\mathcal{R}_0}$, $\mathcal{O}_{{\mathcal{L}_0}^2\mathcal{R}_0}$, and $\mathcal{O}_{\mathcal{L}_0{\mathcal{R}_0}^2}$. For the cycles of larger periods these boundaries are the solutions of higher degree polynomials of f_c and f_d.

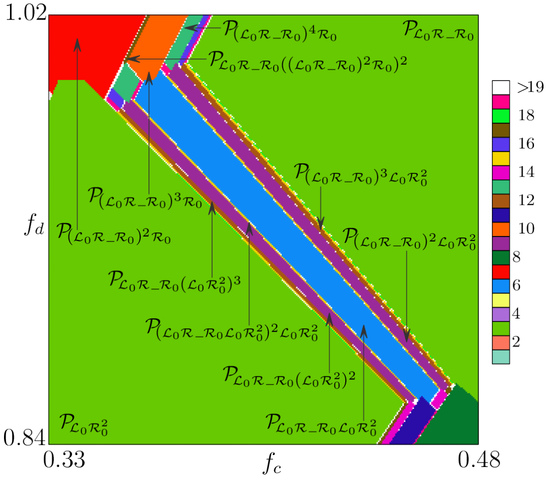

Fig. 5 Period adding structure between periodicity regions $\mathcal{P}_{\mathcal{L}_0{\mathcal{R}_0}^2}$ and $\mathcal{P}_{\mathcal{L}_0\mathcal{R}_-\mathcal{R}_0}$ in the (f_c, f_d) parameter plane for $b = 0.64, d_1 = 0.2, d_2 = 0.1$ and $a = 0.73$.

As we have already shown, two boundaries of $\mathcal{P}_{\mathcal{L}_0{\mathcal{R}_0}^2}$ correspond to the BC conditions

$$X_{\mathcal{L}_0{\mathcal{R}_0}^2} = 0 \quad \text{and} \quad X_{\mathcal{R}_0\mathcal{L}_0\mathcal{R}_0} = 0. \tag{29}$$

The third boundary is related to the collision of $(X_{{\mathcal{R}_0}^2\mathcal{L}_0}, X_{\mathcal{L}_0{\mathcal{R}_0}^2})$ with B_-, that is, to the condition

$$X_{\mathcal{L}_0{\mathcal{R}_0}^2} = X_{{\mathcal{R}_0}^2\mathcal{L}_0} - 1. \tag{30}$$

The region $\mathcal{P}_{\mathcal{L}_0\mathcal{R}_-\mathcal{R}_0}$ related to the complementary cycle $\mathcal{O}_{\mathcal{L}_0\mathcal{R}_-\mathcal{R}_0}$ is also observed and is confined by the BC boundaries related to the conditions

$$X_{\mathcal{L}_0\mathcal{R}_-\mathcal{R}_0} = 0, \quad X_{\mathcal{R}_0\mathcal{L}_0\mathcal{R}_-} = 0, \quad \text{and} \quad X_{\mathcal{L}_0\mathcal{R}_-\mathcal{R}_0} = X_{\mathcal{R}_-\mathcal{R}_0\mathcal{L}_0} - 1. \tag{31}$$

Both bifurcation boundaries, related to $(X_{{\mathcal{R}_0}^2\mathcal{L}_0}, X_{\mathcal{L}_0{\mathcal{R}_0}^2}) \in B_-$ (30) and $(X_{\mathcal{R}_-\mathcal{R}_0\mathcal{L}_0}, X_{\mathcal{L}_0\mathcal{R}_-\mathcal{R}_0}) \in B_-$ (the last equation of (31)), lead to another period adding structure based on the symbolic sequences of the cycles $\mathcal{O}_{\mathcal{L}_0{\mathcal{R}_0}^2}$ and $\mathcal{O}_{\mathcal{L}_0\mathcal{R}_-\mathcal{R}_0}$. Periodicity regions forming this structure are clearly located in the parameter space between $\mathcal{P}_{\mathcal{L}_0\mathcal{R}_-\mathcal{R}_0}$ and $\mathcal{P}_{\mathcal{L}_0{\mathcal{R}_0}^2}$. Symbolic sequences of the cycles of higher periods are concatenations of $\mathcal{L}_0\mathcal{R}_-\mathcal{R}_0$ and $\mathcal{L}_0\mathcal{R}_0^2$, namely they are $\mathcal{L}_0\mathcal{R}_-\mathcal{R}_0(\mathcal{L}_0\mathcal{R}_0^2)^j$ and $(\mathcal{L}_0\mathcal{R}_-\mathcal{R}_0)^j\mathcal{L}_0\mathcal{R}_0^2$, $j = 1, 2, \ldots$.

The same regularity is also observed between two disjoint regions related to cycles of different periods. For example, between $\mathcal{P}_{\mathcal{L}_0\mathcal{R}_-\mathcal{R}_0}$ and the region $\mathcal{P}_{(\mathcal{L}_0\mathcal{R}_-\mathcal{R}_0)^2\mathcal{R}_0}$ associated with a cycle of period seven, there exists a period adding structure based on the two respective symbolic sequences. Namely, it is composed by the regions $\mathcal{P}_{(\mathcal{L}_0\mathcal{R}_-\mathcal{R}_0)^j(\mathcal{L}_0\mathcal{R}_-\mathcal{R}_0)^2\mathcal{R}_0}$ and $\mathcal{P}_{\mathcal{L}_0\mathcal{R}_-\mathcal{R}_0((\mathcal{L}_0\mathcal{R}_-\mathcal{R}_0)^2\mathcal{R}_0)^j}$, $j = 1, 2, \ldots$, associated with cycles of periods $7 + 3j$ and $3 + 7j$. Similarly, between the region $\mathcal{P}_{\mathcal{L}_0\mathcal{R}_-\mathcal{R}_0(\mathcal{L}_0\mathcal{R}_-\mathcal{R}_0)^2\mathcal{R}_0}$ corresponding to period ten and $\mathcal{P}_{\mathcal{L}_0\mathcal{R}_0{}^2}$ there exists a period adding structure based on the sequences $\sigma_1 = \mathcal{L}_0\mathcal{R}_-\mathcal{R}_0(\mathcal{L}_0\mathcal{R}_-\mathcal{R}_0)^2\mathcal{R}_0$ and $\sigma_2 = \mathcal{L}_0\mathcal{R}_0^2$.

For a different parameter constellation (i.e., for $a = 1.15$ as in Fig. 3(b)), regions related to two complementary cycles can overlap, such as $\mathcal{P}_{\mathcal{R}_0\mathcal{L}_0{}^2}$ and $\mathcal{P}_{\mathcal{R}\mathcal{L}_+\mathcal{L}_0}$. Similarly, the regions related to different periods belonging to two distinct period adding structures may overlap pairwise, as for example for $a = 0.73$, the regions $\mathcal{P}_{\mathcal{L}_0\mathcal{R}_0{}^2}$ and $\mathcal{P}_{(\mathcal{L}_0\mathcal{R}_-\mathcal{R}_0)^2\mathcal{R}_0}$, $\mathcal{P}_{(\mathcal{L}_0\mathcal{R}_-\mathcal{R}_0)^3\mathcal{R}_0}$ and $\mathcal{P}_{\mathcal{L}_0\mathcal{R}_-\mathcal{R}_0\mathcal{L}_0\mathcal{R}_0{}^2}$, $\mathcal{P}_{(\mathcal{L}_0\mathcal{R}_-\mathcal{R}_0)^4\mathcal{R}_0}$ and $\mathcal{P}_{(\mathcal{L}_0\mathcal{R}_-\mathcal{R}_0)^2\mathcal{L}_0\mathcal{R}_0{}^2}$, etc (see Fig. 5). In all these cases, two different attracting cycles coexist in the state space.

4.3 Periodicity regions related to 2-cycles

As we have already mentioned, the regions related to cycles of period two are particular. First, there are two respective regions, $\mathcal{P}_{\mathcal{L}_0\mathcal{R}_0}$ and $\mathcal{P}_{\mathcal{L}_+\mathcal{R}_-}$, associated with symbolic sequences that differ for two letters (not a single one). Second, between $\mathcal{P}_{\mathcal{L}_0\mathcal{R}_0}$ and $\mathcal{P}_{\mathcal{L}_+\mathcal{R}_-}$ there exists a particular patchwork-like bifurcation structure, all regions of which are related to cycles of even periods (see Fig. 6). As shown below, some of the periodicity regions belonging to this bifurcation structure are organized according to the period adding principle, and ordering of the others correspond to period incrementing. Recall that period incrementing bifurcation structure is represented by an infinite sequence of (usually) pairwise overlapping periodicity regions related to cycles with periods n_i forming an arithmetic series $n_i = n_0 + i\Delta n$, $i \geq 0$, $\Delta n \geq 1$ (see, e.g., [39] and references therein).

The major reason why a cycle of period two is different from the others, is that its points are always symmetric with respect to the main diagonal $Y = X$. Indeed, for any $\mathcal{O}_{s_1s_2} = \{(X_1, Y_1), (X_2, Y_2)\}$, $s_i \in \{\mathcal{L}_-, \mathcal{L}_0, \mathcal{L}_+, \mathcal{R}_-, \mathcal{R}_0, \mathcal{R}_+\}$, $i = 1, 2$ there is $Y_2 = X_1$ and $Y_1 = X_2$, i.e., $\mathcal{O}_{s_1s_2} = \{(X_1, X_2), (X_2, X_1)\}$. Due to this property, the admissible symbolic sequences for cycles of period two are $\mathcal{L}_0^2$, $\mathcal{R}_0^2$, $\mathcal{L}_0\mathcal{R}_0$, $\mathcal{L}_-\mathcal{L}_+$, $\mathcal{R}_-\mathcal{R}_+$, and $\mathcal{L}_+\mathcal{R}_-$. It is easy to show further that the cycles $\mathcal{O}_{\mathcal{L}_0{}^2}$, $\mathcal{O}_{\mathcal{R}_0{}^2}$, $\mathcal{O}_{\mathcal{L}_-\mathcal{L}_+}$, and $\mathcal{O}_{\mathcal{R}_-\mathcal{R}_+}$ can be only virtual. Therefore, the only admissible 2-cycles are $\mathcal{O}_{\mathcal{L}_0\mathcal{R}_0}$ and $\mathcal{O}_{\mathcal{L}_+\mathcal{R}_-}$, for which the two respective periodicity regions are observed in the (f_c, f_d) parameter plane for $a < 1$.

The boundaries of the region $\mathcal{P}_{\mathcal{L}_0\mathcal{R}_0}$, issuing from the point $(f_c, f_d) = (0, 0)$ are given by the conditions $X_{\mathcal{L}_0\mathcal{R}_0} = 0$ and $X_{\mathcal{R}_0\mathcal{L}_0} = 0$. The third boundary is related to the collision $(X_{\mathcal{L}_0\mathcal{R}_0}, X_{\mathcal{R}_0\mathcal{L}_0}) \in B_+$, or equivalently $X_{\mathcal{R}_0\mathcal{L}_0} = X_{\mathcal{L}_0\mathcal{R}_0} + 1$. On the other hand, the same condition means $X_{\mathcal{L}_0\mathcal{R}_0} = X_{\mathcal{R}_0\mathcal{L}_0} - 1$, and hence, $(X_{\mathcal{R}_0\mathcal{L}_0}, X_{\mathcal{L}_0\mathcal{R}_0}) \in B_-$, i.e., both points of the cycle collide simultaneously with the respective switching manifold each. This corresponds to a so-called nonregular BCB. Similarly, three boundaries of $\mathcal{P}_{\mathcal{L}_+\mathcal{R}_-}$ are defined by the conditions $X_{\mathcal{L}_+\mathcal{R}_-} = 0$, $X_{\mathcal{R}_-\mathcal{L}_+} = 0$, and $X_{\mathcal{R}_-\mathcal{L}_+} = X_{\mathcal{L}_+\mathcal{R}_-} + 1$, the latter being the same as $X_{\mathcal{L}_+\mathcal{R}_-} = X_{\mathcal{R}_-\mathcal{L}_+} - 1$.

Nonregularity of two BCBs of the cycles $\mathcal{O}_{\mathcal{L}_0\mathcal{R}_0}$ and $\mathcal{O}_{\mathcal{L}_+\mathcal{R}_-}$ related to the switching manifolds $B_\pm$ leads to a particular bifurcation structure located between the regions $\mathcal{P}_{\mathcal{L}_0\mathcal{R}_0}$ and $\mathcal{P}_{\mathcal{L}_+\mathcal{R}_-}$. Roughly speaking, this structure is mostly confined whithin a quadrangle Q with vertices in points $A = (a +$

$d_2, 1)$, $B = (1, b + d_2)$, $C = (a + d_1, 1)$, and $D = (1, b + d_1)$. However, some regions slightly overhang the area Q leading to coexistence of the respective 2-cycle (either $\mathcal{O}_{\mathcal{L}_0\mathcal{R}_0}$ or $\mathcal{O}_{\mathcal{L}_+\mathcal{R}_-}$) with the cycles of larger period. The symbolic sequences related to this bifurcation structure are based on the combinations of four pairs: $\mathcal{L}_0\mathcal{R}_0$, $\mathcal{L}_+\mathcal{R}_-$, $\mathcal{L}_+\mathcal{R}_0$, and $\mathcal{L}_0\mathcal{R}_-$, among which two latter sequences correspond to 2-cycles that are always virtual.

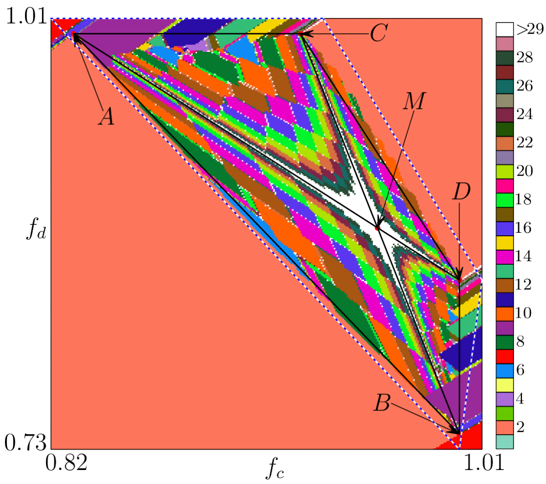

Fig. 6 The bifurcation structure between periodicity regions $\mathcal{P}_{\mathcal{L}_0\mathcal{R}_0}$ and $\mathcal{P}_{\mathcal{L}_+\mathcal{R}_-}$ in the (f_c, f_d) parameter plane for $b = 0.64, d_1 = 0.2, d_2 = 0.1$ and $a = 0.73$.

To describe this bifurcation structure, it is convenient to consider separately four triangular subareas AMB, CMD, AMC, and BMD, where M is the intersection of the lines AD and BC (see Fig. 6). The ordering principle of the periodicity regions inside each subarea is similar but based on different combinations of symbolic pairs. Let us consider the subarea AMB, where symbolic sequences are based on three pairs $\mathcal{L}_0\mathcal{R}_0$, $\mathcal{L}_+\mathcal{R}_0$, and $\mathcal{L}_0\mathcal{R}_-$. The cycle of the smallest period six is $\mathcal{O}_{\mathcal{L}_0\mathcal{R}_0\mathcal{L}_+\mathcal{R}_0\mathcal{L}_0\mathcal{R}_-}$ (see also Fig. 7 where the area Q is shown magnified). The respective periodicity region begins a sequence of regions accumulating towards the point M. For the sake of brevity, let us call them *central regions*. Their ordering correspond to the period incrementing bifurcation structure with periods $4n + 2$, $n \geq 1$, and the neighbor regions overlap pairwise. On the other hand, the related symbolic sequences are $\mathcal{L}_0\mathcal{R}_0(\mathcal{L}_+\mathcal{R}_0)^n(\mathcal{L}_0\mathcal{R}_-)^n$, which differ a bit from what one typically observes in bifurcation structures of such kind. Symbolic sequences of cycles involved in the period incrementing structure are expected to be given as $\sigma_1\sigma_2^n$ with some primary σ_1 and σ_2. Here instead, there are three primary sequences $\sigma_1 = \mathcal{L}_0\mathcal{R}_0$, $\sigma_2 = \mathcal{L}_+\mathcal{R}_0$, and $\sigma_3 = \mathcal{L}_0\mathcal{R}_-$ that are concatenated according to the rule $\sigma_1\sigma_2^n\sigma_3^n$.

As the next step, we describe two groups of regions distributed along the line AB at both sides of $\mathcal{P}_{\mathcal{L}_0\mathcal{R}_0\mathcal{L}_+\mathcal{R}_0\mathcal{L}_0\mathcal{R}_-}$. At first, let us focus on the larger regions associated with periods $6 + 2m$, $m \geq 1$. We call them regions of the first tier. For increasing f_d (decreasing f_c), the related symbolic sequences are $\rho_m := \mathcal{L}_0\mathcal{R}_-\mathcal{L}_0\mathcal{R}_0(\mathcal{L}_+\mathcal{R}_0)^{m+1}$ (with $\rho_0 := \mathcal{L}_0\mathcal{R}_-\mathcal{L}_0\mathcal{R}_0\mathcal{L}_+\mathcal{R}_0$), so that the regions $\mathcal{P}_{\rho_m}$, $m \geq 0$ represent the part of the period adding structure of the first complexity level. Between any two (disjoint) neighbor regions $\mathcal{P}_{\rho_m}$ and $\mathcal{P}_{\rho_{m+1}}$ there exist regions of the second complexity level related to symbolic sequences $\rho_m\rho_{m+1}^k$ and $\rho_m^k\rho_{m+1}$, $k \geq 1$. And between any two neighbor regions of the second complexity level there are regions of the third comlexity level, and so on ad infinitum. In such a way, the ordering of the regions located to the left of $\mathcal{P}_{\mathcal{L}_0\mathcal{R}_0\mathcal{L}_+\mathcal{R}_0\mathcal{L}_0\mathcal{R}_-}$ (for increasing f_d and decreasing f_c) corresponds to the period adding structure built on the sequences $\sigma_1 = \mathcal{L}_0\mathcal{R}_-\mathcal{L}_0\mathcal{R}_0$ and $\sigma_2 = \mathcal{L}_+\mathcal{R}_0$, related to the part of the basic regions $\mathcal{P}_{\sigma_1\sigma_2^{m+1}}$, $m \geq 0$.

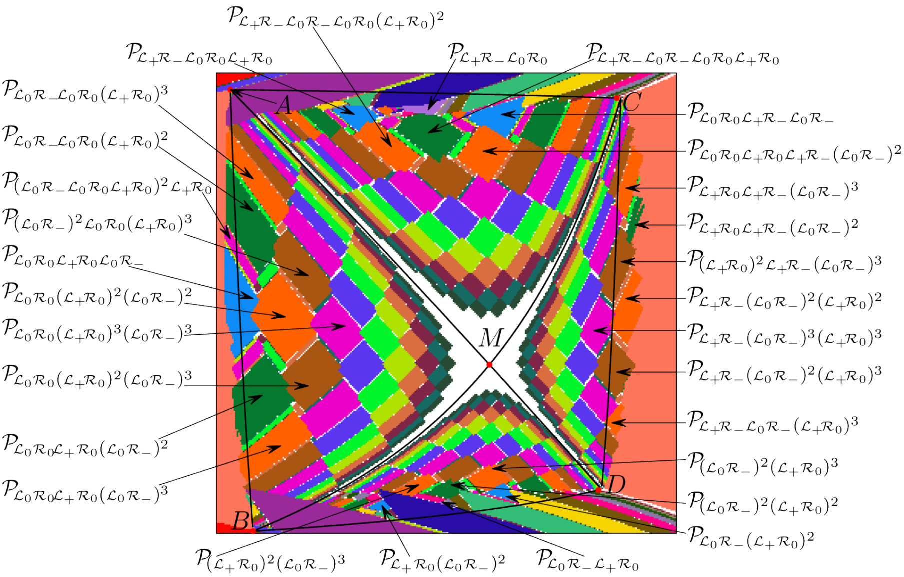

Fig. 7 Magnification of the quadrangular area marked in Fig. 6 by the dashed blue line.

For decreasing f_d (increasing f_c), the regions are ordered according to the same principle, that is, related to the basic regions $\mathcal{P}_{\sigma_1\sigma_2^{m+1}}$, $m \geq 0$ of the period adding structure, but with $\sigma_1 = \mathcal{L}_0\mathcal{R}_0\mathcal{L}_+\mathcal{R}_0$ and $\sigma_2 = \mathcal{L}_0\mathcal{R}_-$. Namely, the regions of the first tier are $\mathcal{P}_{\mathcal{L}_0\mathcal{R}_0\mathcal{L}_+\mathcal{R}_0(\mathcal{L}_0\mathcal{R}_-)^{m+1}}$, and between any two neighbor regions a respective period adding structure is observed.

Similarly, each central region $\mathcal{P}_{\mathcal{L}_0\mathcal{R}_0(\mathcal{L}_+\mathcal{R}_0)^n(\mathcal{L}_0\mathcal{R}_-)^n}$, $n \geq 2$ induces two sequences of regions, which we call the regions of tier n. For increasing f_d and decreasing f_c, the related symbolic sequences are $(\mathcal{L}_0\mathcal{R}_-)^n\mathcal{L}_0\mathcal{R}_0(\mathcal{L}_+\mathcal{R}_0)^{n+m}$, $m \geq 1$, while for decreasing f_d and increasing f_c they are $\mathcal{L}_0\mathcal{R}_0(\mathcal{L}_+\mathcal{R}_0)^n(\mathcal{L}_0\mathcal{R}_-)^{n+m}$. For example, to the left of the region $\mathcal{P}_{\mathcal{L}_0\mathcal{R}_0(\mathcal{L}_+\mathcal{R}_0)^2(\mathcal{L}_0\mathcal{R}_-)^2}$, corresponding to period ten, there are regions

$\mathcal{P}_{(\mathcal{L}_0\mathcal{R}_-)^2\mathcal{L}_0\mathcal{R}_0(\mathcal{L}_+\mathcal{R}_0)^{m+2}}$, and to the right of it there are $\mathcal{P}_{\mathcal{L}_0\mathcal{R}_0(\mathcal{L}_+\mathcal{R}_0)^2(\mathcal{L}_0\mathcal{R}_-)^{m+2}}$. Between any two neighbor regions of tier n (associated with the same central region and forming the first complexity level of the period adding structure), there are regions of higher complexity levels again organized according to the period adding. Two neighbor regions of tiers n and $n+1$ (associated with different central regions) can overlap (as, e.g., $\mathcal{P}_{(\mathcal{L}_0\mathcal{R}_-)^2\mathcal{L}_0\mathcal{R}_0(\mathcal{L}_+\mathcal{R}_0)^3}$ and $\mathcal{P}_{\mathcal{L}_0\mathcal{R}_-\mathcal{L}_0\mathcal{R}_0(\mathcal{L}_+\mathcal{R}_0)^2}$) and can be disjoint. In the latter case, between them another period adding structure is observed. As, for instance, between $\mathcal{P}_{\mathcal{L}_0\mathcal{R}_0(\mathcal{L}_+\mathcal{R}_0)^2(\mathcal{L}_0\mathcal{R}_-)^2}$ and $\mathcal{P}_{\mathcal{L}_0\mathcal{R}_-\mathcal{L}_0\mathcal{R}_0(\mathcal{L}_+\mathcal{R}_0)^2}$ one observes the regions related to periods 18, 26, and 28. Or between $\mathcal{P}_{(\mathcal{L}_0\mathcal{R}_-)^2\mathcal{L}_0\mathcal{R}_0(\mathcal{L}_+\mathcal{R}_0)^3}$ and $\mathcal{P}_{\mathcal{L}_0\mathcal{R}_-\mathcal{L}_0\mathcal{R}_0(\mathcal{L}_+\mathcal{R}_0)^3}$ there is a region corresponding to a 22-cycle.

Let us now turn to the subarea CMD. The main organization principle of the preiodicity regions is the same as in the subarea AMB, but now the primary symbolic pairs are $\mathcal{L}_+\mathcal{R}_-$, $\mathcal{L}_+\mathcal{R}_0$, and $\mathcal{L}_0\mathcal{R}_-$. The central regions are $\mathcal{P}_{\mathcal{L}_+\mathcal{R}_-(\mathcal{L}_0\mathcal{R}_-)^n(\mathcal{L}_+\mathcal{R}_0)^n}$ with $n \geq 2$. Then there are regions of tiers n $\mathcal{P}_{(\mathcal{L}_+\mathcal{R}_0)^n\mathcal{L}_+\mathcal{R}_-(\mathcal{L}_0\mathcal{R}_-)^{n+m}}$ and $\mathcal{P}_{\mathcal{L}_+\mathcal{R}_-(\mathcal{L}_0\mathcal{R}_-)^n(\mathcal{L}_+\mathcal{R}_0)^{n+m}}$, $n \geq 1$, $m \geq 1$. Note that the central region with $n = 1$ related to the 6-cycle is not visible, though the associated sequences of regions of the first tier are observable (for instance, $\mathcal{P}_{\mathcal{L}_+\mathcal{R}_0\mathcal{L}_+\mathcal{R}_-(\mathcal{L}_0\mathcal{R}_-)^2}$ and $\mathcal{P}_{\mathcal{L}_+\mathcal{R}_0\mathcal{L}_+\mathcal{R}_-(\mathcal{L}_0\mathcal{R}_-)^3}$ associated with periods 8 and 10, respectively). Two neighbor regions belonging to different tiers can overlap or can be disjoint. In the latter case, as well as in case of two neighbor regions belonging to the same tier, there exists a respective period adding structure.

The organizing principle of the bifurcation structures in the subareas AMB and CMD can be summarized as follows. The symbolic sequences are based on three primary pairs σ_1, σ_2, σ_3. For AMB there are $\sigma_1 = \mathcal{L}_0\mathcal{R}_0$, $\sigma_2 = \mathcal{L}_+\mathcal{R}_0$, $\sigma_3 = \mathcal{L}_0\mathcal{R}_-$, while for CMD there are $\sigma_1 = \mathcal{L}_+\mathcal{R}_-$, $\sigma_2 = \mathcal{L}_0\mathcal{R}_-$, $\sigma_3 = \mathcal{L}_+\mathcal{R}_0$. The sequences related to regions of the first complexity level are constructed according to the rules $\sigma_3^n\sigma_1\sigma_2^{n+m}$ and $\sigma_1\sigma_2^n\sigma_3^{n+m}$, $n \geq 1$, $m \geq 0$. And between two disjoint regions of the first complexity level there exist regions of higher complexity levels organized according to the period adding principle.

In the subarea AMC, all four primary pairs $\mathcal{L}_0\mathcal{R}_0$, $\mathcal{L}_+\mathcal{R}_-$, $\mathcal{L}_+\mathcal{R}_0$, and $\mathcal{L}_0\mathcal{R}_-$ are involved in formation of symbolic sequences. The cycle with smallest period four is $\mathcal{O}_{\mathcal{L}_+\mathcal{R}_-\mathcal{L}_0\mathcal{R}_0}$. The related region is the first in the sequence of central regions $\mathcal{P}_{\mathcal{L}_+\mathcal{R}_-(\mathcal{L}_0\mathcal{R}_-)^n\mathcal{L}_0\mathcal{R}_0(\mathcal{L}_+\mathcal{R}_0)^n}$, $n \geq 0$, which accumulate towards the point M. The region $\mathcal{O}_{\mathcal{L}_+\mathcal{R}_-\mathcal{L}_0\mathcal{R}_0}$ also starts two sequences of regions of the first tier, associated with the symbolic sequences $\mathcal{L}_+\mathcal{R}_-\mathcal{L}_0\mathcal{R}_0(\mathcal{L}_+\mathcal{R}_0)^m$, $m \geq 0$ for decreasing f_c and $\mathcal{L}_0\mathcal{R}_0\mathcal{L}_+\mathcal{R}_-(\mathcal{L}_0\mathcal{R}_-)^m$ for increasing f_c. Similarly, any central region $\mathcal{P}_{\mathcal{L}_+\mathcal{R}_-(\mathcal{L}_0\mathcal{R}_-)^n\mathcal{L}_0\mathcal{R}_0(\mathcal{L}_+\mathcal{R}_0)^n}$, $n \geq 1$ starts two sequences of regions of tier $n+1$. Namely, for decreasing f_c, the regions $\mathcal{P}_{\mathcal{L}_+\mathcal{R}_-(\mathcal{L}_0\mathcal{R}_-)^n\mathcal{L}_0\mathcal{R}_0(\mathcal{L}_+\mathcal{R}_0)^{n+m}}$ and for increasing f_c, the regions $\mathcal{P}_{\mathcal{L}_0\mathcal{R}_0(\mathcal{L}_+\mathcal{R}_0)^n\mathcal{L}_+\mathcal{R}_-(\mathcal{L}_0\mathcal{R}_-)^{n+m}}$, $m \geq 0$. Between any pair of neighbor regions belonging to the same tier, as well as between any pair of disjoint neighbor regions belonging to the adjacent tiers, a respective period adding structure exists. The regions belonging to the adjacent tiers can also overlap.

In the subarea BMD, the bifurcation structure is based on only two primary pairs $\mathcal{L}_0\mathcal{R}_-$ and $\mathcal{L}_+\mathcal{R}_0$. The central regions are $\mathcal{P}_{(\mathcal{L}_0\mathcal{R}_-)^n(\mathcal{L}_+\mathcal{R}_0)^n}$, $n \geq 1$. The regions of the first tier (associated with the region $\mathcal{P}_{\mathcal{L}_0\mathcal{R}_-\mathcal{L}_+\mathcal{R}_0}$ corresponding to period four) are $\mathcal{P}_{\mathcal{L}_0\mathcal{R}_-(\mathcal{L}_+\mathcal{R}_0)^{m+1}}$ and $\mathcal{P}_{\mathcal{L}_+\mathcal{R}_0(\mathcal{L}_0\mathcal{R}_-)^{m+1}}$, $m \geq 0$. The regions of tier n are, respectively, $\mathcal{P}_{(\mathcal{L}_0\mathcal{R}_-)^n(\mathcal{L}_+\mathcal{R}_0)^{n+m}}$ and $\mathcal{P}_{(\mathcal{L}_+\mathcal{R}_0)^n(\mathcal{L}_0\mathcal{R}_-)^{n+m}}$. As inside all other subareas, two neighbor regions can overlap if they belong to different tiers. If they are disjoint (as always happens when they belong to the same tier), a respective period adding structure is observed in between.

4.4 Economic functioning of the deterministic exchange rate model

From an economic perspective we can say that a cycle permits to obtain from the deterministic model the alternation of bull and bear phases typical of the exchange rate market. In particular, when the time period is high, the time series is hardly distinguishable from a chaotic one, so not easy learnt from traders. Fig. 8 shows the timeseries of X and $X - Y$ for a combination of parameters such that a cycle of high period is the attractor. We have also added a third timeseries to better understand how the dynamics takes place. We plot the net value of the excess demands of fundamentalists and chartists of kind 1 (i.e., $aX - f_c$ or $bX + f_d$), and the excess demand of chartists of kind 2 (i.e., $d_iX^2 - d_iXY$ or $-d_iX^2 + d_iXY$). When the net value of the excess demands of fundamentalists and chartists of kind 1 has the same sign as the excess demand of chartists of kind 2, we sum up them and represent it as a red rectangle. In this case, the exchange rate will strongly move in a certain direction in the next period. When they have opposite sign, we plot in black the net excess demand of fundamentalists and chartists of kind 1, while we plot in blue the excess demand of chartists of kind 2. In this case, they behave differently and what happens to the exchange rate in the next period depends on the largest between the two. As we can see from these timeseries, when the buying pressure prevails, like at the beginning of the series, in the next period the exchange rate reaches a peak. However, at a certain moment the exchange rate becomes so much higher than its fundamental value that the selling pressure becomes the most relevant and the exchange rate has a drop. Then the sequence starts again. Each of these phases may last more than one period. This kind of fluctuations persists over time producing the alternation of bull and bear periods. In our opinion, the introduction of a stochastic element to the model (that can be interpreted as the presence of noise traders) can permit to replicate more quantitative features of real exchange rate markets. This is what we do in the next section.

5 Stochastic model

In this section we exploit the dynamics of the stochastic setting of the model to investigate the extent to which our model is able to replicate the statistical

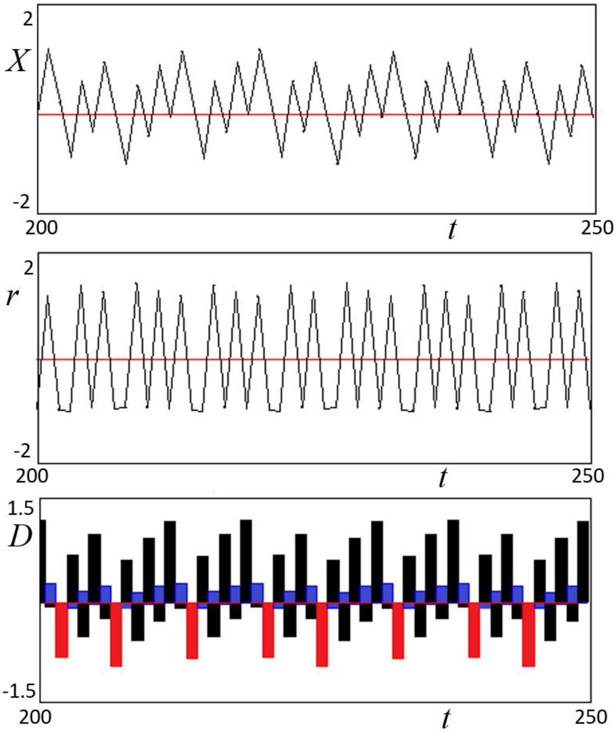

Fig. 8 Example of 50 periods simulated timeseries obtained with the same parameters' configuration used for the previous figures and $f_c = 0.906$ and $f_d = 1.161$. The panel at the top shows the timeseries of X, the one in the middle the timeseries of $X - Y$ (i.e. returns), while the one at the bottom represents the weights of the excess demands of the three kinds of traders. Red rectangles represent periods where the net excess demand of fundamentalists and chartists of kind 1 and the excess demand of chartists of kind 2 behave at the same way (they both buy or sell). When they behave defferently their excess demands are represented in black for the net excess demand value of fundamentalists and chartists of kind 1, and in blue for chartists of kind 2.

properties of the exchange rate movements. In what follows, we rely on the works of [4, 5].

The dataset used in this paper is extracted from Datastream and covers the period from January 2003 until November 2022 (5191 daily observations for each index). The simulations are performed taking into account the analysis of the deterministic skeleton of the model perturbed by a stochastic component, i.e., an independent and normally distributed random variable ε_t. In this respect, the resulting map becomes:

$$T := \begin{cases} X' &= f(X,Y) + \varepsilon_t \quad \text{with} \qquad \varepsilon_t \sim N(0, (\sigma_\varepsilon)^2), \\ Y' &= X. \end{cases} \tag{32a}$$

Table 1 Summary statistics for EUR/USD, EUR/JPY, Sim Model A, and Sim-Model B. The table reports the summary statistics including minimum (r_{min}) and maximum (r_{max}) exchange rate returns, standard deviation (sd), skewness, kurtosis, Jarque-Bera statistic (J-B statistic), the characteristic exponent (ζ), the Hurst exponent for exchange returns (H_r) and absolute exchange returns ($H_{|r|}$), respectively.

	EUR/USD	EUR/JPY	Sim-Model A	Sim-Model B
r_{min}	-0.0332	-0.0896	-0.0607	-0.0620
r_{max}	0.0381	0.0864	0.0592	0.06075
sd	0.0059	0.0073	0.0130	0.0129
Skewness	0.0306	-0.4235	-0.1644	-0.0937
Kurtosis	5.1720	16.32	4.726	4.861
J-B statistic	1021.6	38552	12865	14569
ζ	4.08	4.275	3.876	3.856
H_r	0.5403	0.5405	0.5051	0.5148
$H_{\|r\|}$	0.7301	0.7581	0.7015	0.7269

We consider the following parameter set: $f_c = 0.014$; $f_d = 0.011$; $b = 0.64$; $d_1 = 0.2$; $d_2 = 0.1$, $a = 0.73$, $\sigma_\varepsilon = 0.07$. The value σ_ε is a positive parameter indicating the standard deviations of the normal random variable, chosen in order to match the path of the actual exchange rates. As we already said, it can easily be interpreted as the addition of noise traders into the picture. In what follows, we concentrate our attention on the log exchange rate defined as $r_t = \ln(X_t) - \ln(X_{t-1})$. We run the model for 10000 periods, focusing on the last 5191 periods. In Table 1 we provide some useful summary statistics for EUR/USD, EUR/JPY, Sim-Model A and Sim-Model B exchange rate returns.

Panels (a) and (d) of Fig. 9 confirm that exchange rate returns alternate periods of low volatility with periods of high volatility demonstrating the presence of volatility clustering. Indeed, we can observe that the exchange rate returns deviate from their fundamental value in all the markets and exhibit irregular fluctuations that range between -0.03 to 0.04 for EUR/USD, between -0.09 and 0.09 for EUR/JPY, between -0.06 and 0.06 for Sim-Model A, and between -0.06 and 0.06 for Sim-Model B. A simple inspection of Table 1 suggests that, in terms of skewness, our model is closely related to the EUR/JPY index. Indeed, in Sim-Model A, Sim-Model B and EUR/JPY the skewness is negative and equal to -0.1644, -0.0937 and -0.4235, respectively. This implies that extreme and negative exchange rate returns are more probable than positive ones, and it is also a signal that the distribution of exchange rate returns is not normal. Unlike Sim-Model A, Sim-Model B and EUR/JPY, EUR/USD displays a skewness slightly above zero. In addition, to confirm that the distribution of the exchange rate returns of our model is not normal, we provide several other statistics.

First, we report the results of the Jarque-Bera test for all the three models (see the values of the statistic in the J-B statistic column of Table 1). According to this test, under the null hypothesis exchange rate returns follow a normal distribution, otherwise their distribution is not normal. In Table 1, the Jarque-Bera test rejects the null hypothesis at the 1% significant level given that, for all the models, the J-B statistic is greater than the critical value of 5.8461. In panels (b), (e) of Fig. 9, plotted are the probability density functions of

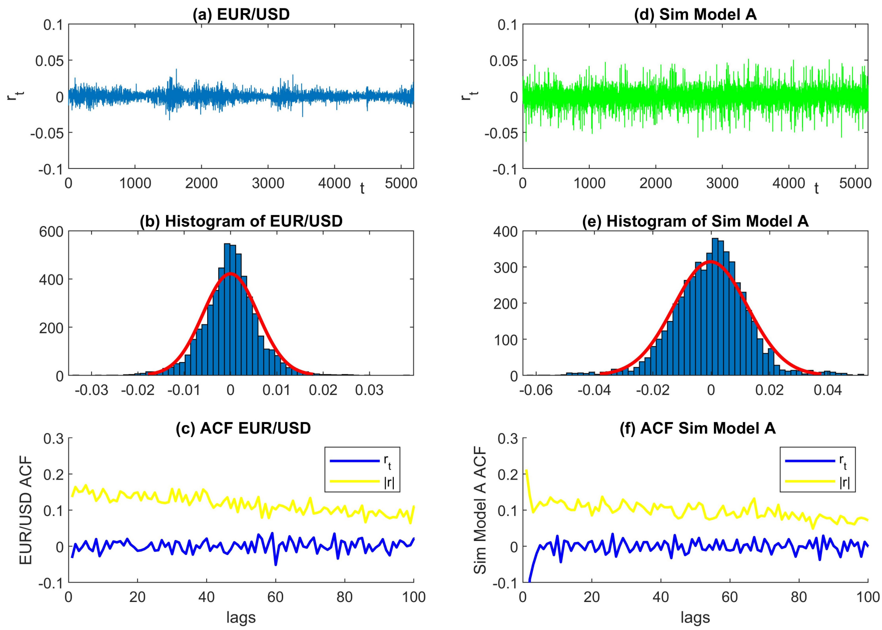

Fig. 9 Exchange rate returns series (panel (a)), distribution of the exchange rate returns (panel (b)) and autocorrelation function of raw and absolute exchange rate returns (panel (c))for EUR/USD for time periods $t \in [2003, 2022]$. The same diagrams are figured in panels (d)-(f) for Sim Model A, respectively.

exchange rate returns compared to that of the Normal distribution (depicted by the red solid line). We observe that our model replicates quite well the distribution of the exchange rate returns of the EUR/USD. Indeed, we can see that the most part of the mass is in the peak and tails are comparable to the case of a Normal distribution. This fact is also confirmed by an excess of kurtosis of 4.726 for Sim-Model A, and 5.1720 for EUR/USD indicating that the distribution of the exchange rate returns is leptokurtic, i.e., it has heavy tails. Finally, we employ the Hill tail index estimator (see the values reported in the ζ column of Table 1) to analyse the tailedness of the empirical distribution of the exchange rate returns. We obtain that the tail index of our model (equal to 3.876 for Sim-Model A, and 3.856 for Sim-Model B) is coherent with those of EUR/USD and EUR/JPY which exhibit a ζ of 4.08 and 4.275, respectively.

In line with [4, 5], we find evidence of absence of autocorrelation in the exchange rate return series, while there is persistence of autocorrelation in the absolute exchange rate return series, as shown in Fig. 9 panels (c), (f). This stylized fact is known as long memory effect. In the third row of Fig. 9 plotted are the autocorrelation functions (ACFs) for returns (in blue) and absolute returns (in yellow) with respect to the first 100 lags. It is evident that, for all the three models, the ACFs of absolute exchange rate returns are persistent also after 100 lags while the ACFs of exchange rate returns are insignificant after the first few lags. This phenomenon is also captured by the Hurst exponent of absolute exchange rate returns (reported in the last column of Table 1) which ranges between 0.70 and 0.75, confirming a slow decay of the ACFs of absolute returns similar to a hyperbolic function.

6 Conclusion

In this paper, we sought to connect to the growing literature on heterogeneous agent models in the exchange rate market which proved to be able to replicate important features of this particular market. Our work aims at contributing in the exploitation of the power of nonlinear trading rules combined with switching regimes typical of the behavioral literature. Our nonlinear piecewise-defined model permits to qualitatively replicate the fluctuations of real markets, already in its deterministic skeleton. We performed a deep analytical and numerical analysis of the shapes of the periodicity regions in the parameter space, showing that periodic motion (of basically any periodicity) is the most typical outcome of the model and a small change in the value of a behavioral parameter may drastically change the periodicity.

We have described three different parts of the overall bifurcation structure in the parameter space. The first part is located in the neighborhood of an organizing center associated with a continuity breaking bifurcation. It is characterized by an infinite number of BCB curves issuing from a single point and the periodicity regions close to this point are ordered according to the period adding structure. For the parameter values being sufficiently distant from this organizing center, there may exist other period adding structures, each being placed between two disjoint periodicity regions related to cycles having the same period but associated with symbolic sequences that differ by one letter. Two neighbor regions belonging to two different period adding structures may overlap or may be disjoint, in which case another period adding structure exists in between. Finally, between the regions associated with period two, there may exist a particular patchwork-like bifurcation structure related to cycles of even periods. We have shown that some of periodicity regions belonging to this structure are organized according to the period adding, and ordering of the others correspond to period incrementing principle.

We have also performed some simulations with a stochastic version of our model, finding promising results. In the future we plan to deepen the analysis of the stochastic model by letting the behavioral reactivity parameters change and by introducing more sophisticated statistical and econometrical tools to see how many stylized facts of the exchange rate markets we can replicate. We also want to introduce more behavioral features into the model given the robust findings on it coming from behavioral finance studies. We think that these models may help a policy maker to regulate the market, so we will also try to introduce its role.

Acknowledgements

AP expresses her cordial thanks to colleagues from Urbino and Milan (Italy), Szczecin (Poland) and Lisbon (Portugal) for their support during Russian invasion to Ukraine. AP also acknowledges a partial financial support by the National Academy of Sciences of Ukraine within the scopes of the project "Mathematical modelling of complex dynamical systems and processes caused by the state security" (Reg. No. 0123U100853).

Declarations

Conflict of Interest All authors declare that they have no conflict of interest.

References

[1] Gardini, L., Radi, D., Schmitt, N., Sushko, I., Westerhoff, F.: Currency manipulation and currency wars: Analyzing the dynamics of competitive central bank interventions. Journal of Economic Dynamics and Control **145**, 104545 (2022)

[2] Frankel, J.A., Froot, K.A., *et al.*: Understanding the US dollar in the eighties: the expectations of chartists and fundamentalists. Economic record **62**(1), 24–38 (1986)

[3] De Grauwe, P., Grimaldi, M.: Exchange rate puzzles: a tale of switching attractors. European Economic Review **50**(1), 1–33 (2006)

[4] Manzan, S., Westerhoff, F.: Representativeness of news and exchange rate dynamics. Journal of Economic Dynamics and Control **29**(4), 677–689 (2005)

[5] Manzan, S., Westerhoff, F.H.: Heterogeneous expectations, exchange rate dynamics and predictability. Journal of Economic Behavior & Organization **64**(1), 111–128 (2007)

[6] Menkhoff, L., Taylor, M.P.: The obstinate passion of foreign exchange professionals: technical analysis. Journal of Economic Literature **45**(4), 936–972 (2007)

[7] Federici, D., Gandolfo, G.: The euro/dollar exchange rate: Chaotic or non-chaotic? A continuous time model with heterogeneous beliefs. Journal of Economic Dynamics and Control **36**(4), 670–681 (2012)

[8] De Grauwe, P., Kaltwasser, P.R.: Animal spirits in the foreign exchange market. Journal of Economic Dynamics and Control **36**(8), 1176–1192 (2012)

[9] Goldbaum, D., Zwinkels, R.C.: An empirical examination of heterogeneity and switching in foreign exchange markets. Journal of Economic Behavior & Organization **107**, 667–684 (2014)

[10] Gori, M., Ricchiuti, G.: A dynamic exchange rate model with heterogeneous agents. Journal of Evolutionary Economics **28**, 399–415 (2018)

[11] Campisi, G., Muzzioli, S., Tramontana, F.: Uncertainty about fundamental, pessimistic and overconfident traders: a piecewise-linear maps approach. Decisions in Economics and Finance **44**, 707–726 (2021)

[12] Föllmer, H., Horst, U., Kirman, A.: Equilibria in financial markets with heterogeneous agents: a probabilistic perspective. Journal of Mathematical Economics **41**(1-2), 123–155 (2005)

[13] Gardini, L., Radi, D., Schmitt, N., Sushko, I., Westerhoff, F.: Perception of fundamental values and financial market dynamics: Mathematical insights from a 2d piecewise linear map. SIAM Journal on Applied Dynamical Systems **21**(4), 2314–2337 (2022)

[14] Nusse, H.E., Yorke, J.A.: Border-collision bifurcations including period two to period three for piecewise smooth systems. Phys. D **57**, 39–57 (1992)

[15] Banerjee, S., Karthik, M.S., Yuan, G., Yorke, J.A.: Bifurcations in one-dimensional piecewise smooth maps—theory and applications in switching circuits. IEEE Trans. Circ. Syst. I **47**(3), 389–394 (2000)

[16] Zhusubaliyev, Z.T., Mosekilde, E.: Bifurcations and Chaos in Piecewise-smooth Dynamical Systems. World Scientific, Singapore (2003)

[17] Sushko, I., Agliari, A., Gardini, L.: Bifurcation structure of parameter plane for a family of unimodal piecewise smooth maps: Border-collision bifurcation curves. Chaos Solitons Fract. **29**, 756–770 (2006)

[18] Gardini, L., Avrutin, V., Sushko, I.: Codimension-2 border collision bifurcations in one-dimensional discontinuous piecewise smooth maps. Int. J. Bif. Chaos **24**(2), 1450024 (2014)

[19] Gardini, L., Merlone, U., Tramontana, F.: Inertia in binary choices: continuity breaking and big-bang bifurcation points. J. Econ. Behav. Organization **80**, 153–167 (2011)

[20] Gardini, L., Avrutin, V., Schanz, M., Granados, A., Sushko, I.: Organizing centers in parameter space of discontinuous 1D maps with one increasing and one decreasing branches. In: ESAIM (European Series in Applied and Industrial Mathematics), vol. 36, pp. 106–120 (2012)

[21] Avrutin, V., Schanz, M.: On multi-parametric bifurcations in a scalar piecewise-linear map. Nonlinearity **19**, 531–552 (2006)

[22] Avrutin, V., Schanz, M., Banerjee, S.: Multi-parametric bifurcations in a piecewise–linear discontinuous map. Nonlinearity **19**, 1875–1906 (2006)

[23] Avrutin, V., Schanz, M., Banerjee, S.: Codimension-three bifurcations: Explanation of the complex one-, two-, and three-dimensional bifurcation structures in nonsmooth maps. Phys. Rev. E **75**, 066205 (2007)

[24] Avrutin, V., Granados, A., Schanz, M.: Sufficient conditions for a period incrementing big bang bifurcation in one-dimensional maps. Nonlinearity **24**(9), 2575 (2011)

[25] Leonov, N.N.: Map of the line onto itself. Radiofisika **2**(6), 942–956 (1959)

[26] Keener, J.P.: Chaotic behavior in piecewise continuous difference equations. Trans. Am. Math. Soc. **261**(2), 589–604 (1980)

[27] Homburg, A.J.: Global Aspects of Homoclinic Bifurcations of Vector Fields. Memories of the American Math. Soc., vol. 121. American Math. Soc., Providence, RI (1996)

[28] Tramontana, F., Westerhoff, F., Gardini, L.: On the complicated price dynamics of a simple one-dimensional discontinuous financial market model with heterogeneous interacting traders. J. Econ. Behav. Organization **74**(3), 187–205 (2010)

[29] Tramontana, F., Gardini, L., Westerhoff, F.: Heterogeneous speculators and asset price dynamics: further results from a one-dimensional discontinuous piecewise-linear model. Computational Economics **38**, 329–347 (2011)

[30] Kahneman, D., Tversky, A.: Prospect theory: An analysis of decision under risk. Econometrica **47**(2), 263–291 (1979)

[31] Farebrother, R.W.: Simplified samuelson conditions for cubic and quartic equations. The Manchester School **41**(4), 396–400 (1973)

[32] Gandolfo, G.: Economic Dynamics. Springer, Heidelberg (2010)

[33] Gumovsky, I., Mira, C.: Dynamique Chaotique: Transformations Ponctuelles. Transition Ordre-Désordre. Collection Nabla. Cépaduès Édition, Toulouse (1980)

[34] Mira, C., Gardini, L., Barugola, A., Cathala, J.-C.: Chaotic Dynamics in Two-Dimensional Noninvertible Maps. Nonlinear Science. World Scientific, Singapore (1996)

[35] Abraham, R., Gardini, L., Mira, C.: Chaos in Discrete Dynamical Systems: A Visual Introduction in 2 Dimensions. Springer, New York (1997)

[36] Agliari, A., Bischi, G.I., Gardini, L.: Some methods for the global analysis of dynamic games represented by iterated noninvertible maps. In: Puu, T., Sushko, I. (eds.) Oligopoly Dynamics, pp. 31–83. Springer, Heidelberg (2002)

[37] Gardini, L., Tramontana, F., Avrutin, V., Schanz, M.: Border-collision bifurcations in 1D piecewise-linear maps and Leonov's approach. Int. J. Bif. Chaos **20**(10), 3085–3104 (2010)

[38] Avrutin, V., Schanz, M., Gardini, L.: Calculation of bifurcation curves by map replacement. Int. J. Bif. Chaos **20**(10), 3105–3135 (2010)

[39] Avrutin, V., Gardini, L., Sushko, I., Tramontana, F.: Continuous and Discontinuous Piecewise-smooth One-dimensional Maps: Invariant Sets and Bifurcation Structures. World Scientific, Singapore (2019)